Available online at www.sciencedirect.com
ScienceDirect
Trans. Nonferrous Met. Soc. China 29(2019) 2472−2482
Transactions of Nonferrous Metals Society of China
www.tnmsc.cn

Nondestructive evaluation of mechanical properties of nanostructured Al−Cu alloy at room and elevated temperatures

Hany R. AMMAR[1,2], Fahmy M. HAGGAG[3]

1. Mechanical Engineering Department, College of Engineering, Qassim University, Saudi Arabia;
2. Metallurgical and Materials Engineering Department, Faculty of Petroleum and Mining Engineering, Suez University, Suez, Egypt;
3. ABI Services, LLC, 115 Clemson Drive, Oak Ridge, Tennessee 37830, USA

Received 4 February 2019; accepted 28 October 2019

Abstract: The influence of processing variables on the mechanical properties of a nanostructured Al−10wt.%Cu alloy was investigated. Stress−strain microprobe® system (SSM) and its automated ball indentation® (ABI®) test were used for evaluating the mechanical properties of this alloy. The tests were conducted at 21 °C on the bulk samples that were mechanically alloyed for 6 h at two ball-to-powder mass ratios (BPR) of 30:1 and 90:1. Furthermore, the tests were conducted at 200 and 400 °C on the samples that were processed at BPR of 90:1. Increasing BPR resulted in raising the final indentation load from (316±26) to (631±9) N and reducing the final indentation depth from 111 to 103 μm. Regarding the samples that were processed at BPR of 90:1, increasing the test temperature from 21 to 400 °C resulted in decreasing the final load from (631±9) to (125±1) N and increasing the final depth from 103 to (116±1) μm. The sample processed at BPR of 90:1 and tested at 21 °C revealed the highest strength and the least deformability while the sample processed at BPR of 90:1 and tested at 400 °C exhibited the lowest strength and the greatest deformability, as compared to all samples under study.

Key words: Al−Cu alloy; ball milling; automated ball indentation® (ABI®); mechanical properties; test temperature

1 Introduction

Aluminum alloys are promising materials for industrial applications, as a result of their high specific strength ratio which decreases energy consumption and improves their mechanical performance. Ball milling technique or mechanical alloying method has been used for production of advanced and new Al alloys with enhanced mechanical performance. Several aluminum alloys have already been synthesized by means of ball milling, such as Al−Mg and Al−Zr alloys. Superior strength Al−Ti alloys have also been produced with improved properties even at high-temperature [1,2]. Al−Fe alloys are another series of Al-based alloys with enhanced properties at the room and elevated temperatures [3−6].

Advanced Technology Corporation (ATC) patented a novel nondestructive test system with new technique, namely, stress−strain microprobe (SSM) system and its automated ball indentation (ABI) [7] technique, the main objective of establishing this new technique was the nondestructive determination of the mechanical properties of materials with a miniature size. The SSM−ABI test technique was established according to the well-known and confirmed physical concepts and mathematical correlations which govern the metal behavior [7,8]. SSM−ABI test technique is well-described in several references [7,9−11]. The SSM−ABI test method displays numerous remarkable benefits [12]. These advantages include: using minimal sample size; conducting the test without significant specimen preparation; determining the major mechanical properties at different temperatures in a nondestructive manner; simple and quick test procedures where the overall test is accomplished in few minutes; and the test produces interesting results. Additionally, SSM−ABI test method is widely implemented for nondestructive testing of industrial and engineering components in-service conditions. Furthermore, this test method is used for

Corresponding author: Hany R. AMMAR; E-mail: hanyammar@qec.edu.sa
DOI: 10.1016/S1003-6326(19)65155-1

nondestructive determination of fatigue and creep properties of metallic materials [13]. It was reported that the SSM−ABI test method was successfully applied for determining the key mechanical properties of several metals and alloys. These alloys include iron and steel alloys [14−17], Al alloys [18,19], Ti alloys [20], Zr alloys [21,22] and soldering materials [23,24]. The reported results of these studies confirmed that the SSM−ABI test results were in full agreement with the results obtained from standard mechanical testing techniques.

In the current study, a nanostructured Al−10%Cu alloy was fabricated using powder metallurgy route where mechanical alloying was used to produce the alloy in the powder form, thereafter, sintering was conducted on the alloy powders to develop the bulk solid samples. The applications of traditional mechanical tests such as tensile test are not appropriate in the present study due to the small size (10 mm in diameter and 10 mm in height) of the sintered samples. Consequently, SSM−ABI test was used for evaluating the mechanical properties of the developed alloy at 21, 200 and 400 °C. The data generated from applying the SSM−ABI tests on the samples subjected to various production and testing variables were processed for determining indentation load vs indentation depth curves, stress vs strain curves, ultimate tensile strength, yield strength and ABI hardness.

2 Experimental

Mechanical alloying was employed to synthesize a nanostructured Al−10wt.%Cu alloy. The premixed Al and Cu powders were mechanically alloyed for a period of 6 h of milling with applying two ball-to-powders mass ratios (BPR) of 30:1 and 90:1. The mechanical alloying process was accomplished by means of 1S-attritor. The mechanically alloyed Al−10wt.%Cu powders were sintered into dense bulk specimens by means of high frequency induction heat sintering. The sintering process was performed under 133.3 mPa at 400 °C and 7.35 kN/cm^2 (74 MPa) for a duration of 4 min; with a heating rate of 350 °C/min and a cooling rate of 400 °C/min. X-ray diffraction (XRD) analysis was conducted on the sintered bulk Al−10wt.%Cu alloy specimens which were mechanically alloyed for 6 h at BPR of 30:1 and 90:1. XRD analysis comprises the phase identification and determination of the crystallite size of the sintered bulk samples processed at BPR of 30:1 and 90:1. The morphology and size of the indentation region after conducting the SSM−ABI tests were characterized by means of apreo field emission scanning electron microscope (AFESEM). The actual chemical composition of the sintered alloy was confirmed using AFESEM equipped with energy dispersive X-ray spectroscopy (EDS).

The sintered samples of Al−10wt.%Cu which were processed at BPR of 30:1 and 90:1 were tested at various temperatures using SSM−ABI technique. The sintered sample dimensions were 10 mm in diameter and 10 mm in height. Room temperature tests were conducted on the sintered samples which were processed at BPR of 30:1 and 90:1. Further, SSM−ABI tests were conducted at 200 and 400 °C on the solid bulk samples which were mechanically alloyed at BPR of 90:1. The stress−strain microprobe® (SSM) uses an indenter controlled in an electro-mechanical manner, a load cell, a data-acquisition apparatus, a computer and a copy-righted automated ball indentation® (ABI®). In the current study a spherical indenter from tungsten carbide with a diameter of 0.762 mm was used. The indenter was forced into the sample surface at a rate of 0.02 mm/s. Sequential loading and intermediary partial un-loading cycles were performed at the same location of the tested sample surface where eight cycles of loading and unloading were performed during each test. A load cell and a differential transducer were used for the continuous collection of the load of indentation versus the depth of penetration. In the present study, the SSM−ABI tests were carried out at two locations on each sample, as shown in Fig. 1, to examine the alloy consistency. The size of the samples is small, accordingly, only two SSM−ABI tests were conducted on each sample where each test is equivalent to a tensile test in the fact that continuous load−depth data in the SSM−ABI test are collected versus load−extension data in the tensile test. The locations of the SSM−ABI tests are indicated by numbers 1 and 2 on the sample surface, as shown in Fig. 1. The alloy processing parameters and SSM−ABI test temperatures of the alloy are listed in Table 1.

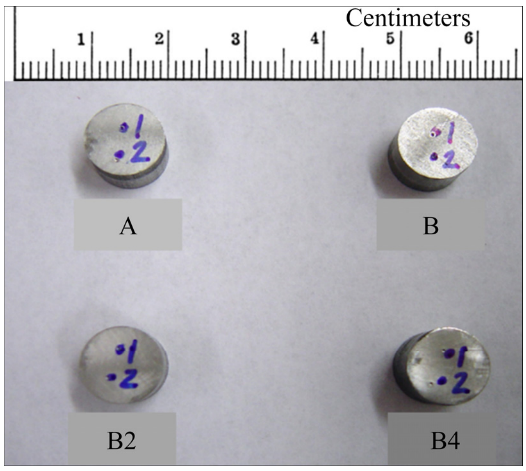

Fig. 1 Locations of SSM−ABI tests performed on samples indicated by numbers 1 and 2 on each sample surface

Table 1 Processing parameters and SSM−ABI test temperatures of alloy

Alloy code	Chemical composition	Milling time/h	Ball-to-powder mass ratio (BPR)	Test temperature/°C
A	Al−10wt.%Cu	6	30:1	21
B	Al−10wt.%Cu	6	90:1	21
B2	Al−10wt.%Cu	6	90:1	200
B4	Al−10wt.%Cu	6	90:1	400

3 SSM−ABI test and data analysis

As mentioned in the previous section, the SSM−ABI testing implies a sphere-shaped indenter to perform a sequential indentation where a definite number of successive loading and intermediary partially un-loading cycles were performed at the same location of the surface of the tested sample with a specific loading rate [7−9]. Regarding each cycle, an indentation load (P) and penetration depth which comprises the total penetration depth (h_t) and plastic penetration depth (h_p) were continuously collected [7−9]. The data from the load of indentation and depth of penetration were collected through the whole SSM−ABI test to plot the load−depth curve [7−9]. The data obtained from SSM−ABI test are used to generate the true stress and true plastic strain curve. With regard to each successive cycle of loading and un-loading, the tested material beneath the indenter exhibited severe plastic deformation with an increase in the depth of indentation which led to concurrent strain hardening and yielding of the material [7−9].

The SSM−ABI test generates a strain of indentation which is estimated by TABOR [25]. This indentation strain is correlated to a true plastic strain (ε_p) in a uniaxial tensile testing through the following correlation:

$$\varepsilon_p=0.2(d_p/D) \tag{1}$$

where D is the indenter diameter and d_p is the plastic indentation diameter. d_p can be calculated by the consequent Hertzian equation [7]:

$$d_p=\sqrt[3]{2.735P\left(\frac{1}{E_1}+\frac{1}{E_2}\right)D\left\{\frac{h_p^2+0.25d_p^2}{h_p^2+0.25d_p^2-h_pD}\right\}} \tag{2}$$

where E_1 is the elasticity modulus of the indenter; E_2 is the elasticity modulus of tested sample; P is the load of indentation. The true stress is estimated by Eq. (3), as follows [7]:

$$\sigma_t=S_m/\delta=4P/\pi d_p^2\delta \tag{3}$$

where S_m is the mean normal pressure, and δ is a factor estimated based on the progress of the plastic region beneath the indenter. The yield strength of tested sample is determined according to converting the final depth of penetration (h_t) into a total diameter of indentation (d_t) for each loading cycle according to the following relationship [7]:

$$d_t=2(h_tD-h_t^2)^{0.5} \tag{4}$$

Linear regression analysis was applied for data fitting from loading cycles to Eq. (5) [7]:

$$P/d_t^2=A(d_t/D)^{m-2} \tag{5}$$

where m is the Meyer's constant, A is a material parameter to be obtained by a regression analysis of P/d_t^2 vs d_t/D, subsequently, the yield strength (σ_y) is determined by [7]

$$\sigma_y=\beta_m A \tag{6}$$

where β_m is a material constant.

The test results data obtained from SSM−ABI test were applied to estimating the exponent of strain hardening (n) and the coefficient of strength (K) from the generated true−stress versus true−plastic-strain curves. These stress−strain curves were fitted to a power law (Eq. (7)) to estimate the values of n and K [8,9]:

$$\sigma_t=K\varepsilon_p^n \tag{7}$$

where σ_t is the true stress.

According to the fact that the flow behavior of metallic samples satisfies the power law (Eq. (7)), consequently, the ultimate tensile strength (UTS, σ_b) can be calculated based on Eq. (8) [8,9]:

$$\sigma_b=K(n/e)^n \tag{8}$$

where e is a dimensionless constant, 2.718.

The data obtained from the SSM−ABI test results were used to calculate the Brinell hardness (HB, H_B) using the following standard (Eq. (9)) [8,9]:

$$H_B=2P_{max}/\{\pi D[D-(D^2-D_f^2)^{0.5}]\} \tag{9}$$

where P_{max} is the final indentation load and D_f is the final indentation diameter. It should be noted that the hardness value from the SSM−ABI test calculated using Eq. (9) is higher than that obtained from the standard hardness tests conducted with a larger indenter diameter which is attributed to the fact that the elastic compression of the indenter in the case of SSM−ABI test, 0.762 mm, is smaller than that of Brinell hardness test indenter (10, 5 or 2.5 mm). However, when comparing the hardness results obtained from testing the samples using the same indenter diameter, these results obviously display the influence of material processing variables and testing parameters on the properties of the samples. The hardness measured from SSM−ABI test is designated as "ABI-0.762 mm-G", where 0.762 mm indicates the diameter of the indenter and "G" refers to the grinding process used in manufacturing the indenter.

4 Results and discussion

XRD analysis was carried out on the sintered Al−10wt.%Cu specimens which were mechanically alloyed for 6 h at BPR of 30:1 and 90:1. XRD analysis comprises the phase identification and determination of the crystallite size of the sintered bulk samples. Figure 2 shows the XRD patterns of the sintered bulk samples of Al−10wt.%Cu alloys A and B which were processed at BPR of 30:1 and 90:1, respectively. From Fig. 2, it may be observed that increasing the BPR from 30:1 to 90:1 resulted in decreasing the crystallite size and increasing the lattice strain, as may be noticed from the peak broadening of the Sample B as compared to that of Sample A. The average crystallite size calculated from XRD main peaks for Samples A and B were (44±5) and (34±7) nm, respectively, while the average estimated lattice strain for Samples A and B were (0.0028±0.0013) and (0.0042±0.0007), respectively. It may be observed that pure copper peaks are not detected, which is an indication to the development of a supersaturated solid solution of Cu in Al matrix in addition to the formation of Al_2Cu intermetallic phase, as identified on the XRD pattern.

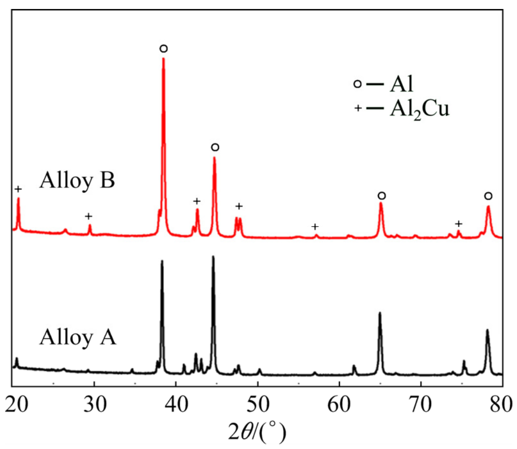

Fig. 2 XRD patterns of sintered bulk samples of Al−10wt.%Cu alloys A and B processed at BPR of 30:1 and 90:1, respectively

4.1 Indentation load−penetration depth behavior

Table 1 summarizes the processing parameters and test conditions of the samples. The processing variables are kept constant except the BPR while the test conditions are kept the same with the exception of the test temperature, as illustrated in Table 1. As mentioned above, the size of the sintered samples are relatively small (10 mm in diameter and 10 mm in height), accordingly, only two SSM−ABI tests were conducted on each sample surface, as illustrated in Fig. 1. SSM−ABI tests were conducted to display the effect of processing and testing variables on the properties of the samples.

Figure 3 shows virtually comparable load of indentation versus depth of indentation curves for Sample A by SSM−ABI tests conducted at 21 °C. It may be observed from Fig. 3 that the average final load of indentation was (316±26) N and the average final depth of penetration was 111 μm. Figure 4 displays similar load versus depth curves for Sample B tested at 21 °C. From Fig. 4, it may be noticed that the average final load of indentation was (631±9) N and the average final depth of penetration was 103 μm. Figure 5 shows a roughly comparable load−depth curves for Sample B2 tested at 200 °C. Regarding Fig. 5, it may be noted that the average final load was 185 N and the average final depth of penetration was (107±1) μm. Figure 6 displays a relatively equivalent load−depth curves for Sample B4 tested at 400 °C. It may be found from Fig. 6 that the average final load was (125±1) N and the average final depth of penetration was (116±1) μm. Figures 3−6 confirm the repeatability of the SSM−ABI tests on the

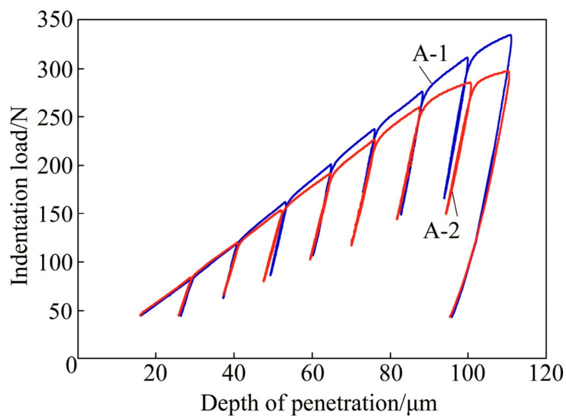

Fig. 3 Virtually comparable load of indentation vs depth of indentation curves for Sample A by SSM−ABI test (A-1 and A-2 refer to positions 1 and 2 on sample surface, shown in Fig. 1)

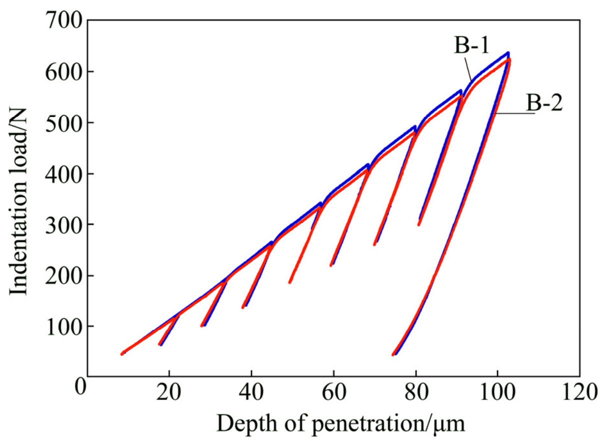

Fig. 4 Similar load of indentation vs depth of indentation curves for Sample B by SSM−ABI test (B-1 and B-2 indicate positions 1 and 2 on sample surface, shown in Fig. 1

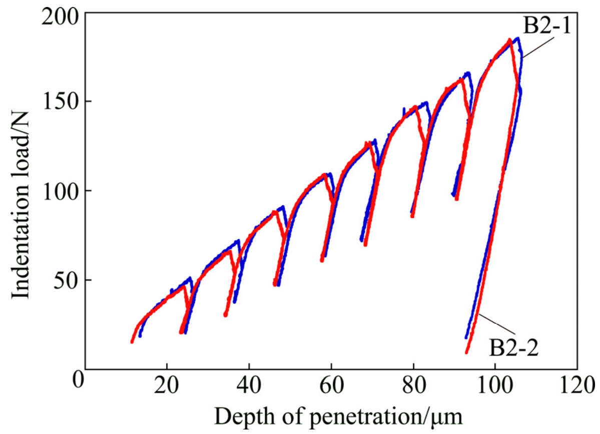

Fig. 5 Roughly comparable load of indentation vs depth of indentation curves for Sample B2 generated by SSM−ABI test (B2-1 and B2-2 refer to positions 1 and 2 on sample surface, shown in Fig. 1)

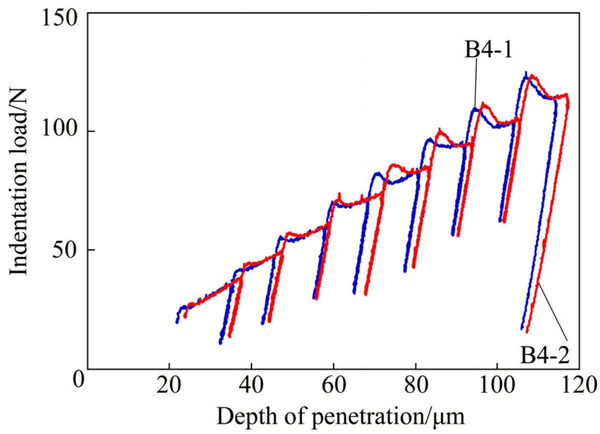

Fig. 6 Relatively equivalent load of indentation vs depth of indentation curves for Sample B4 by SSM−ABI test (B4-1 and B4-2 indicate positions 1 and 2 on sample surface, shown in Fig. 1)

same sample where virtually similar load−depth curves were attained when applying SSM−ABI test on different positions on the same sample. Figure 7 shows a comparison of the load−depth behavior among the samples. The load−depth behavior for each sample in Fig. 7 is presented using one single curve corresponding to one test accomplished on the sample surface (position 1 or 2 in Fig. 1) since Figs. 3−6 conformed the comparable behavior of the two SSM−ABI tests performed on each sample.

Regarding Fig. 7 and comparing the load−depth behavior of Samples A and B, it may be noticed that Sample B revealed larger load of indentation and smaller depth of indentation than Sample A, where the average final load and depth obtained after testing Sample B were (631±9) N and 103 μm, respectively, while the average final load and depth attained after testing Sample A were

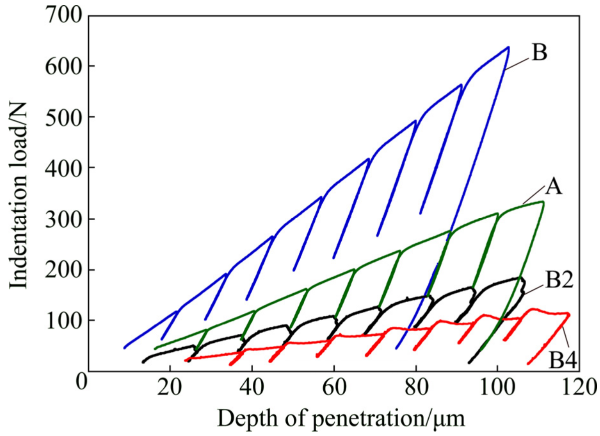

Fig. 7 Indentation load vs indentation depth behaviors of Samples A, B, B2 and B4

(316±26) N and 111 μm, respectively. The difference in the load−depth behavior of Samples A and B is attributed to the difference in the BPR applied during fabrication process. Ball-to-powder mass ratio displays a significant effect on the crystallite size and lattice strain of the processed samples. Increasing the BPR resulted in reducing the crystallite size and increasing the lattice strain in the fabricated samples as well as forming a supersaturated solid solution and precipitating Al_2Cu intermetallic phase, as may be concluded from XRD results shown in Fig. 2. Accordingly, increasing the BPR resulted in increasing the strength and hardness and reducing the deformability of Sample B as compared to Sample A. These are responsible for the increased resistance to penetration and the reduced deformation depth in case of Sample B as compared to Sample A [26,27].

With regard to the load−depth behavior of Samples B, B2 and B4, as presented in Fig. 7, it may be noticed that Sample B exhibited the greatest load of indentation and the lowest depth of indentation as compared to Samples B2 and B4. When increasing the temperature from 21 °C (Sample B) to 200 °C (Sample B2), the final load of indentation was found to decrease significantly from (631±9) to 185 N and the final indentation depth was noticed to increase considerably from 103 to (107±1) μm. A further increase in the temperature to 400 °C (Sample B4) resulted in an additional decrease in the indentation load to reach the minimum value ((125±1) N) of all tested samples and an extra increase in the depth of penetration to display the maximum value ((116±1) μm) of all tested samples. The decrease in the load and the increase in the depth when increasing the test temperature are attributed to the softening phenomena that occur when testing at high temperatures [26,27]. From Fig. 7 it may be concluded that Sample B displayed the highest indentation load and lowest penetration depth while Sample B4 exhibited the lowest load and the highest depth.

4.2 Stress−strain behavior

According to the fundamentals of the SSM−ABI test and data analysis which described in Section 4, the SSM−ABI test results presented in Figs. 3−6 are treated to produce the stress−strain curves for the samples. Figure 8 displays a relatively comparable stress−strain curves for Sample A, and the yield strength determined by SSM−ABI test is the lowest stress in the curves. Regarding Fig. 8, the average yield strength of the two tests conducted on Sample A is (247±28) MPa. Figure 9 illustrates an almost similar stress−strain curves for Sample B where the average yield strength of the two tests is (522±15) MPa. Figure 10 reveals roughly comparable stress−strain curves for Sample B2. In this case, the average yield strength is (134±2) MPa. Figure 11 reveals relatively equivalent stress−strain curves for Sample B4. It can be seen from Fig. 11 that the average yield strength is (82±1) MPa.

Figure 12 displays a comparison of the flow behavior of the samples; however, one stress−strain curve for each sample was presented in this figure since the results shown in Figs. 8−11 reveal relatively equivalent flow curves of the two SSM−ABI tests performed on each sample. With regard to the effect of BPR on the flow behavior of Samples A and B, as shown in Fig. 12, it may be observed that Sample B exhibited higher strength and lower deformability than Sample A where the average yield strength of Sample B was (522±15) MPa, as compared to that of Sample A ((247±28) MPa). Samples A and B are tested at 21 °C; however, this behavior is due to the different BPR used during fabrication of these samples. Increasing the BPR from 30:1 (Sample A) to 90:1 (Sample B) resulted in decreasing the grain size and increasing the lattice strain in addition to the formation of a supersaturated solid solution of Cu in Al and also the precipitation of Al_2Cu intermetallic phases, as noticed from Fig. 2. Consequently, Sample B displayed improved strength and

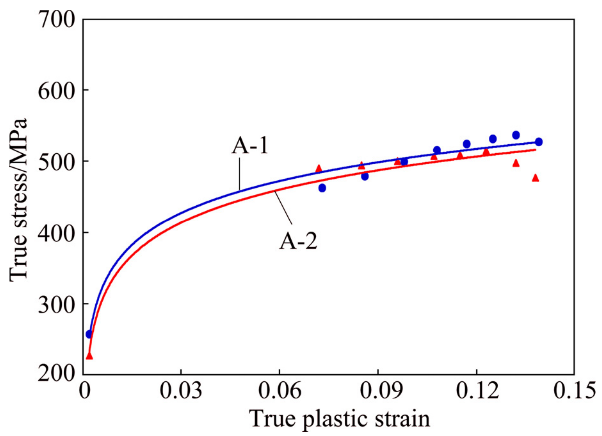

Fig. 8 Relatively comparable stress−strain curves for Sample A by SSM−ABI test (A-1 and A-2 refer to positions 1 and 2 on sample surface, shown in Fig. 1)

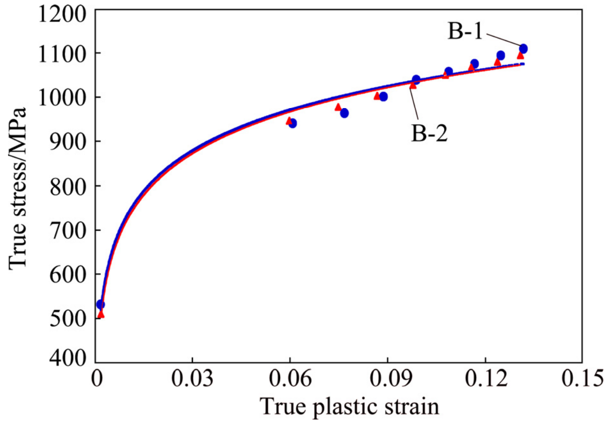

Fig. 9 Almost similar stress−strain curves for Sample B by SSM−ABI test (B-1 and B-2 indicate positions 1 and 2 on sample surface, shown in Fig. 1)

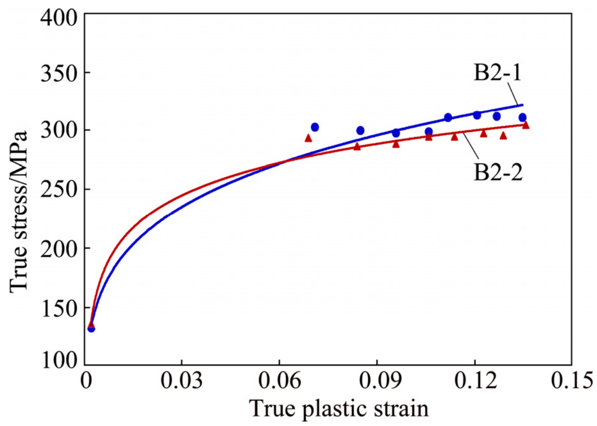

Fig. 10 Roughly comparable stress−strain curves for Sample B2 by SSM−ABI test (B2-1 and B2-2 refer to positions 1 and 2 on sample surface, shown in Fig. 1)

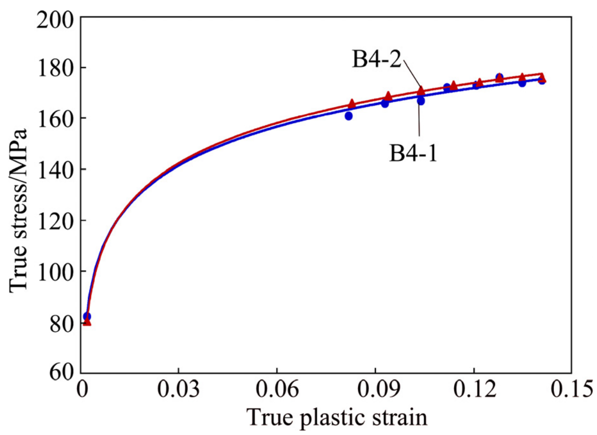

Fig. 11 Relatively equivalent stress−strain curves for Sample B4 by SSM−ABI test (B4-1 and B4-2 indicate positions 1 and 2 on sample surface, shown in Fig. 1)

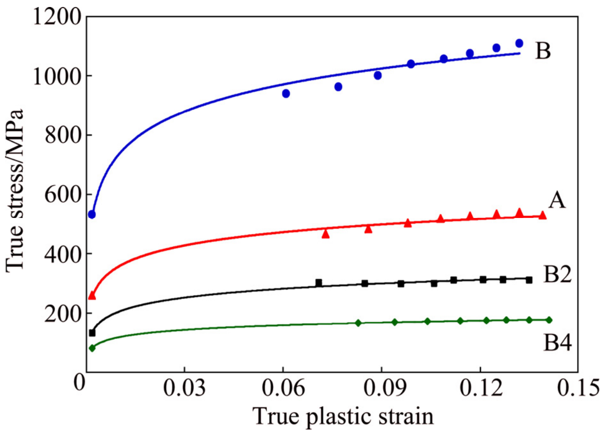

Fig. 12 Behavior of stress−strain curves of Samples A, B, B2 and B4

reduced deformability, as compared to Sample A [26,27]. Furthermore, increasing the temperature resulted in deteriorating the material strength and improving its deformability, as may be seen in Fig. 12 where the yield strength was observed to decrease from (522±15) MPa (Sample B) to (134±2) MPa (Sample B2) and an additional decrease to (82±1) MPa when increasing the test temperature to 400 °C (Sample B4). The reduction in sample strength with raising temperature is ascribed to the softening mechanism at high temperatures [26,27]. It may be concluded from Fig. 12 that Sample B revealed the highest strength while Sample B4 displayed the lowest strength. These results of the flow behavior of the samples are in accordance with those shown in Figs. 3−7.

4.3 Precision and repeatability of SSM−ABI test results

Table 2 lists a summary of the SSM−ABI test results obtained in the present study. These results comprise the average values of final indentation load, final indentation depth, yield strength, ultimate tensile strength, ABI-0.762 mm-G hardness, exponent of strain hardening, and coefficient of strength. It should be noted that Section 4 described the principles of determining these properties.

The average values of ultimate tensile strength (UTS) of the tested samples are listed in Table 2. Regarding the effect of BPR on UTS of Samples A and B which were tested at room temperature, it may be noticed that Sample B revealed larger UTS value of (961±3) MPa than Sample A which exhibited a value of (462±1) MPa. With regard to the effect of temperature on UTS of Sample B, increasing the temperature to 200 °C (Sample B2) resulted in a significant decrease in the UTS from (961±3) to (283±5) MPa. More increase in the temperature to 400 °C (Sample B4) resulted in an additional deterioration of the UTS value which decreased to (156±1) MPa.

With regard to the average hardness values listed in Table 2, it may be observed that increasing the BPR from

Table 2 Summary of key properties obtained from SSM−ABI tests for samples in this study

Tested sample	Final indentation load/N	Final depth of penetration/ μm	Strain hardening exponent, n	Strength coefficient, K/MPa	Yield strength/ MPa	Ultimate tensile strength/ MPa	ABI hardness-0.762 mm-G
A-1	334	111	0.165	735	266	463	130
A-2	298	111	0.193	768	227	461	116
Average	316	111	0	752	247	462	123
Standard deviation	25.5	0.0	0.0	23.3	27.6	1.4	9.9
B-1	637	103	0.172	1543	532	959	265
B-2	625	103	0.181	1572	511	963	259
Average	631	103	0	1558	522	961	262
Standard deviation	8.5	0.0	0.0	20.5	14.8	2.8	4.2
B2-1	185	107	0.209	489	132	286	75
B2-2	185	106	0.197	468	135	279	75
Average	185	107	0	479	134	283	75
Standard deviation	0.0	0.7	0.0	14.8	2.1	4.9	0.0
B4-1	125	115	0.180	252	82	155	43
B4-2	124	117	0.187	259	81	157	42
Average	125	116	0	256	82	156	43
Standard deviation	0.7	1.4	0.0	4.9	0.7	1.4	0.7

30:1 (Sample A) to 90:1 (Sample B) and conducting the test at room temperature resulted in an increase in the hardness value from (123±10) (Sample A) to (262±4) (Sample B). Raising the temperature from room temperature (Sample B) to 200 °C (Sample B2) resulted in deteriorating the hardness value from (262±4) to 75, respectively. An additional increase in the temperature to 400 °C (Sample B4) led to a further diminution in the hardness value to (43±1).

Regarding the results presented in Figs. 3−12 and listed in Table 2, it may be concluded that the SSM−ABI test results of the samples are in a full agreement in displaying the effect of fabrication conditions (BPR) and testing temperatures on the mechanical properties of the samples. These comprise load−depth behavior, stress−strain curves, yield strength, UTS, and ABI-0.762 mm-G hardness. Increasing the BPR from 30:1 (Sample A) to 90:1 (Sample B) resulted in increasing the load of indentation, reducing the indentation depth, improving the yield strength and enhancing the UTS and augmenting the hardness. These experimental results are in accordance with the well-established practice and principles of materials science and engineering.

An increase in the temperature from 21 (Sample B) to 400 °C (Sample B4) resulted in a significant decrease in the indentation load, a considerable increase in the indentation depth, a noticeable deterioration in the yield strength, a substantial decrease in the UTS and an obvious reduction in the hardness. These experimental results are in a full agreement with the fundamentals of materials engineering practice. The attained results in Samples B, B2 and B4 are related to the activated softening mechanisms when increasing the temperature where dislocation mobility is unhindered, as a result of the grain growth, diminishing the lattice strain and the coarsening effect of the Al_2Cu hardening phases which reduced their density and increased their particle size.

From the results obtained in the current study, it may be noticed that the SSM−ABI test clearly revealed the influence of fabrication variables (BPR) and testing temperatures on the mechanical properties of the samples. In addition, the results in the present study exhibited high precision and repeatability where each sample provided almost similar results for the two SSM−ABI tests performed on its surface, as shown in Figs. 3−6 and 8−11.

With regard to the results shown in Table 2, the average and standard deviations were calculated for the two SSM−ABI tests conducted on each sample. The SSM−ABI test is equivalent to a tensile test in the fact that continuous load−depth data in the SSM−ABI test are collected versus load−extension data in the tensile test. However, it would be appropriate that if the statistical sample size for each condition was at least three-to-five tests instead of two in the current case which is considered a small statistical sample size. An average can be accepted but a standard deviation is meaningless for two tests only. The precision of the SSM−ABI test was proven in a study conducted by six laboratories under ASTM and the draft test method and its interlaboratory study (ILS) results are available [28]. Generally, the SSM−ABI test displays high precision value of ±2% (1.5% for yield strength and 1.4% for ultimate tensile strength) [28]. The high precision of this test method is due to its rigidity of the tungsten carbide indenter, the ultra-precision of the two sensors of force and depth, and the use of 16-bit data acquisition system which resulted in minimizing experimental errors and led to a significant repeatability and precision values [28]. The precision values reported in Ref. [28] are based on the results of 120 ABI® tests conducted by six organizations on two steel alloys and two aluminum alloys.

Regarding the test result precision and repeatability it should be highlighted that in the present study the average crystallite sizes calculated from XRD data for Samples A and B were (44±5) and (34±7) nm, respectively. SSM−ABI tests were conducted using an indenter with 0.762 mm in diameter. This indenter covers thousands of grains in the size range of ((44±5)−(34±7) nm), therefore, the test generated reasonable results representing the bulk behavior of the tested samples, which is relatively similar to tensile testing results.

The SSM−ABI technique revealed a reasonable effectiveness in evaluating the flow properties of iron-based alloys [14−17], aluminum alloys [18,19], titanium alloys [20], and zirconium alloys [21,22]. These studies reported the SSM−ABI test results with high precision and repeatability.

The indentation region of Samples B and B4 were examined by means of AFESEM. These two samples were selected for this examination since Sample B displayed the highest strength and the greatest resistance to penetration of all examined samples while Sample B4 exhibited the lowest strength and the least resistance to deformation of all investigated specimens. The characterization comprises the final impression diameter and the material-pile-up surrounding the indentation region. Furthermore, EDS quantitative analysis was applied to determining the sample elemental composition.

Figures 13 (a) and (b) reveal the impression region at one SSM−ABI test location on the Samples B and B4, respectively. It may be noticed that the measured final impression diameter of Sample B ((477±4) μm) was smaller than that of Sample B4 ((589±3) μm). In addition, the material-pile-up around the indentation

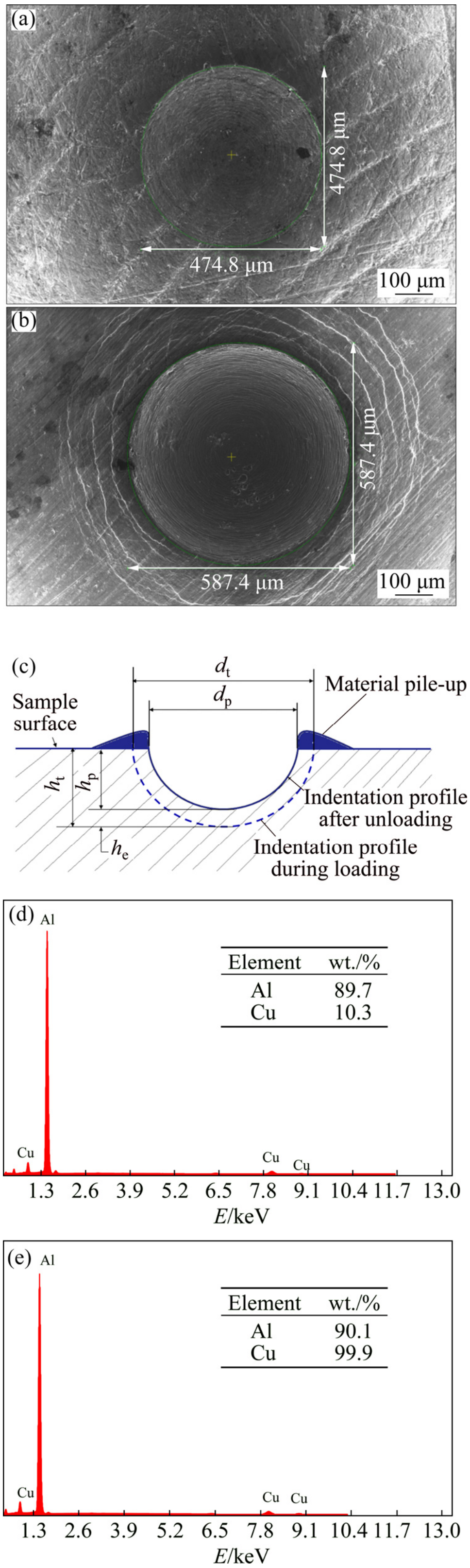

Fig. 13 Secondary electron images displaying final impression size and morphology of Samples B (a) and B4 (b), respectively, schematic representation of geometry of indentation area during loading−unloading cycle of SSM−ABI test (c), EDS quantitative analyses (d, e) of elements existing in collected areas in images (a) and (b), respectively

region is obviously larger in the case of Sample B4 as compared to that of Sample B. These remarks are in agreement with the results presented in this study which concluded that Sample B exhibited the highest strength and the greatest deformation resistance, as compared to Sample B4. Furthermore, the indentation area in Sample B4 clearly revealed the softening effect occurred during the test at elevated temperature as proven by the large diameter and depth of indentation and the extensive pile-up occurred in the region of impression. Figure 13(c) displays a schematic representation of the geometry of the indentation area during loading−unloading cycle of SSM−ABI test. This figure illustrates the total depth of penetration which includes elastic depth and plastic depth in addition to the diameters of the total indentation and plastic indentation. Figures 13(d) and (e) illustrate the EDS quantitative analysis carried out on the indentation region where the elemental composition of the samples was almost Al−10wt.%Cu.

5 Conclusions

(1) Increasing the BPR from 30:1 to 90:1 resulted in increasing the final load of indentation from (316±26) to (631±9) N, reducing the final indentation depth from 111 microns to 103 μm, improving the yield strength from (247±28) to (522±15) MPa, enhancing the UTS from (462±1) to (961±3) MPa and augmenting the ABI hardness from (123±10) to (262±4).

(2) Increasing the temperature from 21 °C (Sample B) to 400 °C (Sample B4) resulted in decreasing the final indentation load from (631±9) to (125±1) N, increasing the final indentation depth from 103 μm to (116±1) μm, deteriorating the yield strength from (522±15) to (82±1) MPa, decreasing the UTS from (961±3) to (156±1) MPa and reducing the ABI hardness from (262±4) to (43±1).

(3) The sample processed at BPR of 90:1 and tested at 21 °C revealed the highest strength and the least deformability while the sample processed at BPR of 90:1 and tested at 400 °C exhibited the lowest strength and the greatest deformability, as compared to all samples.

(4) The result revealed a successful application of the stress−strain microprobe and the automated ball indentation test on determining the mechanical properties of nanostructured Al−10wt.%Cu in a nondestructive manner.

(5) The SSM−ABI tests revealed high precision and repeatability on displaying the effect of BPR and testing temperature on the mechanical properties of the samples.

Acknowledgments

The authors gratefully acknowledge Qassim University, represented by the College of Engineering, on the material support for this research. The authors are also appreciative to ABI Services, LLC for conducting the Automated Ball Indentation (ABI) tests.

References

[1] LEE Kwang-min, MOON In-hyung. High temperature performance of dispersion-strengthened A1−Ti alloys prepared by mechanical alloying [J]. Materials Science and Engineering A, 1994, 185: 165−170.

[2] LERF R, MORRIS D G. Mechanical alloying of Al−Ti alloys [J]. Materials Science and Engineering A, 1990, 128(1): 119−127.

[3] SHAW L, LUO H, VILLEGAS J, MIRACLE D. Thermal stability of nanostructured $Al_{93}Fe_3Cr_2Ti_2$ alloys prepared via mechanical alloying [J]. Acta Materialia, 2003, 51: 2647−2663.

[4] SASAKI T T, OHKUBO T, HONO K. Microstructure and mechanical properties of bulk nanocrystalline Al−Fe alloy processed by mechanical alloying and spark plasma sintering [J]. Acta Materialia, 2009, 57: 3529−3538.

[5] SASAKI T T, MUKAI T, HONO K. A high-strength bulk nanocrystalline Al−Fe alloy processed by mechanical alloying and spark plasma sintering [J]. Scripta Materialia, 2007, 57: 189−192.

[6] KRASNOWSKI M, KULIK T. Nanocrystalline and amorphous Al−Fe alloys containing 60%−85% of Al synthesized by mechanical alloying and phase transformations induced by heating of milling products [J]. Materials Chemistry and Physics, 2009, 116: 631−637.

[7] HAGGAG F M. Field indentation microprobe for structural integrity evaluation: U.S. Patent, 4852397 [P]. 1989-08-01.

[8] HAGGAG F M. In-situ measurements of mechanical properties using novel automated ball indentation system, in small specimen test techniques applied to nuclear reactor thermal annealing and plant life extension [C]//ASTM STP 1204. Philadelphia: American Society for Testing and Materials, 1993: 27−44.

[9] HAGGAG F M, NANSTAD R K, HUTTON J T, THOMAS D L, SWAIN R L. Use of automated ball indentation testing to measure flow properties and estimate fracture toughness in metallic materials, in applications of automation technology to fatigue and fracture testing [C]//ASTM STP 1092. Philadelphia: American Society for Testing and Materials, 1990: 188−208.

[10] HAGGAG F M, WONG H, ALEXANDER D J, NANSTAD R K. The use of field indentation microprobe in measuring mechanical properties of welds, in recent trends in welding science and technology [C]//Proceedings of the 2nd International Conference on Trends in Welding Research. Gatlinburg, Tennessee: ASM, 1989: 843−849.

[11] HAGGAG F M. Application of flow properties microprobe to evaluate gradients in weldment properties [C]//Proceedings of the ASM 3rd International Conference on Trends in Welding Research. Gatlinburg, Tennessee: ASM, 1992: 629−635.

[12] HAGGAG F M, WANG J A. Nondestructive detection and assessment of damage in aging aircraft using a novel stress-strain microprobe system [J]. SPIE, 1996, 2945: 217−228.

[13] HAGGAG F M, MURTY K L. A novel stress-strain microprobe for nondestructive evaluation of mechanical properties of materials [C]// Nondestructive Evaluation and Materials Properties III. The Minerals, Metals & Materials Society, 1997: 101−106.

[14] MALOW T R, KOCH C C, MIRAGLIA P Q, MURTY K L. Compressive mechanical behavior of nanocrystalline Fe investigated with an automated ball indentation technique [J]. Materials Science and Engineering A, 1998, 252: 36−43.

[15] DIPILKA R B, BALLA A R, PESHWE D R, GANESHKUMAR J, LAHA K, MATHEW M D. A study on the effect of tempering temperature on tensile properties of P92 steel by automated ball indentation technique [J]. Procedia Engineering, 2014, 86: 910−918.

[16] NAGARAJU S, GANESHKUMAR J, VASANTHARAJA P, VASUDEVAN M, LAHA K. Evaluation of strength property variations across 9Cr−1Mo steel weld joints using automated ball indentation (ABI) technique [J]. Materials Science and Engineering: A, 2017, 695: 199−210.

[17] HAMADA A S, HAGGAG F M, PORTER D A. Non-destructive determination of the yield strength and flow properties of high-manganese twinning-induced plasticity steel [J]. Materials Science and Engineering A, 2012, 558: 766−770.

[18] PATIL D C, DAS M, DAS G, KORI S A, VENKATESWARLU K. Evaluating the mechanical properties of HPT processed aluminium alloys using automated ball-indentation technique [J]. Procedia Materials Science, 2014, 5: 379−386.

[19] AMMAR H R, HAGGAG F M, ALABOODI A S, AL-MUFADI F A. Nondestructive measurements of flow properties of nanocrystalline Al−Cu−Ti alloy using automated ball indentation (ABI) technique [J]. Materials Science and Engineering A, 2018, 729(27): 477−486.

[20] WANG F, ZHAO J, ZHU N, LI Z. A comparative study on Johnson-Cook constitutive modeling for Ti−6Al−4V alloy using automated ball indentation (ABI) technique [J]. Journal of Alloys and Compounds, 2015, 633: 220−228.

[21] KULKARNI R V, MANI KRISHNA K V, NEOGY S, SRIVASTAVA D, RAMADASAN E, DEY G K, SAIBABA N, JHA S K, SHRIWASTAW R S, ANANTHARAMAN S. Determination of correlation parameters for evaluation of mechanical properties by small punch test and automated ball indentation test for Zr−2.5% Nb pressure tube material [J]. Nuclear Engineering and Design, 2013, 265: 1101−1112.

[22] SHARMA K, SINGH P K, BHASIN V, VAZE K K. Application of automated ball indentation for property measurement of degraded Zr2.5Nb [J]. Journal of Minerals and Materials Characterization and Engineering, 2011, 10(7): 661−669.

[23] MAHIDHARA R K, SASTRY S M L, JERINA K L, TURLIK I, MURTY K L. Room temperature tensile properties of Sn−5%Pb solder [J]. Journal of Materials Science Letters, 1994, 13(19): 1387−1389.

[24] MURTY K L, HAGGAG F M. Characterization of strain-rate sensitivity of Sn−5%Sb solder using ABI testing [J]. The Minerals, Metals & Materials Society, 1996: 37−44.

[25] TABOR D. The hardness of metals [M]. Oxford: Clarendon Press, 1951.

[26] AMMAR H R, KALIL A K, SHERIF E M. Thermally stable nanocrystalline aluminum alloys processed by mechanical alloying and high frequency induction heat sintering [J]. International Journal of Chemical, Molecular, Nuclear, Materials and Metallurgical Engineering, 2015, 9(1): 154−164.

[27] BAIG M, AMMAR H R, SEIKH A H. Thermo-mechanical responses of nanocrystalline Al−Fe alloy processed using mechanical alloying and high frequency heat induction sintering [J]. Materials Science and Engineering A, 2016, 655: 132−141.

[28] HAGGAG F M. In-situ measurement of pipeline mechanical properties using stress-strain microprobe-validation of data for increased confidence & accuracy[R]. A report submitted to Pipeline Research Council International, Inc. Catalog No. L52280, 2007.

纳米结构 Al−Cu 合金
室温和高温力学性能的无损评价

Hany R. AMMAR[1,2], Fahmy M. HAGGAG[3]

1. Mechanical Engineering Department, College of Engineering, Qassim University, Saudi Arabia;
2. Metallurgical and Materials Engineering Department,
Faculty of Petroleum and Mining Engineering, Suez University, Suez, Egypt;
3. ABI Services, LLC, 115 Clemson Drive, Oak Ridge, Tennessee 37830, USA

摘　要：研究工艺参数对纳米结构 Al−10wt.%Cu 合金力学性能的影响。用应力−应变 Microprobe®系统(SSM) 和自动球压痕仪(ABI®)评估合金的力学性能。对于球磨 6 h、球料比(BPR)分别为 30:1 和 90:1 条件下制备的样品，测试温度为 21 °C。此外，还对球料比为 90:1 球磨后制备的样品分别在 200 和 400 °C 下进行高温测试。 结果表明，球料比增加导致最终压痕载荷从(316±26) N 增加到(631±9) N，压痕深度从 111 μm 减小到 103 μm。对于球料比为 90:1 制备的样品， 测试温度从 21 °C 升高到 400 °C，导致最终载荷从(631±9) N 降低到(125±1) N，最终压痕深度从 103 μm 降低到(116±1) μm。在所有测试样品中，球料比为 90:1 制备的样品，当测试温度为 21 °C 时表现出最高的强度和最低的变形能力，而测试温度为 400 °C 时表现出最低的强度和最高的变形能力。

关键词：Al−Cu 合金；球磨；自动球压痕仪®(ABI®)；力学性能；测试温度

(Edited by Xiang-qun LI)